separations

MDPI

Article

Iron Recovery from Turkish and Romanian Bauxite Residues Through Magnetic Separation: Effect of Hydrothermal Processing and Separation Conditions

Panagiotis Angelopoulos *, Paschalis Oustadakis, Nikolaos Kountouris, Michail Samouhos, Georgios Anastassakis and Maria Taxiarchou

School of Mining and Metallurgical Engineering, National Technical University of Athens, 9 Heroon Polytechniou Str., Zografos, 157 80 Athens, Greece; oustadak@metal.ntua.gr (P.O.); nkountouris@metal.ntua.gr (N.K.); msamouhos@metal.ntua.gr (M.S.); ganastas@metal.ntua.gr (G.A.); taxiarh@metal.ntua.gr (M.T.)
* Correspondence: pangelopoulos@metal.ntua.gr; Tel.: +30-210-772-2252

Abstract

This study investigates the potential of two low-iron-grade bauxite residue (BR) samples, containing up to 27.4 wt.% Fe and originating from alumina plants in Romania and Turkey, for the recovery of iron concentrate via wet magnetic separation. The methodology involved the hydrothermal reduction of the residues, aiming to transform the hematite/goethite (Fe^{3+}) phases into magnetite (Fe^{2+}/Fe^{3+}) and enhance their magnetic susceptibility. The effect of hydrothermal treatment, magnetic induction value (up to 1600 Gs), and slurry dispersion on iron recovery and iron grade were investigated. An optimum magnetic fraction was obtained, containing 44.4 wt.% elemental iron (Fe_{elem}) and achieving 98% iron recovery. These results demonstrate a significant improvement compared to the magnetic fraction derived from the respective non-reduced sample, which showed a maximum of 29.7 wt.% Fe grade and 59.7% recovery. Furthermore, silicon and sodium are primarily distributed in the non-ferrous fraction. The application of sonication to enhance slurry dispersion during magnetic separation did not have a positive impact on the process. In addition to iron recovery, an aspect of considerable potential is the reutilization of the Al-rich liquor generated during hydrothermal treatment of the BR. Its reintroduction into the Bayer process circuit could contribute to improved material utilization and enhanced overall process efficiency.

Keywords: bauxite residue; hydrothermal reduction; magnetic separation; iron oxides; sonification

check for updates

Academic Editors: Lihui Gao, Daoguang Teng, Shulei Li and Chunlin He

Received: 1 August 2025
Revised: 9 September 2025
Accepted: 11 September 2025
Published: 17 September 2025

Citation: Angelopoulos, P.; Oustadakis, P.; Kountouris, N.; Samouhos, M.; Anastassakis, G.; Taxiarchou, M. Iron Recovery from Turkish and Romanian Bauxite Residues Through Magnetic Separation: Effect of Hydrothermal Processing and Separation Conditions. *Separations* **2025**, *12*, 252. https://doi.org/10.3390/separations12090252

Copyright: © 2025 by the authors. Licensee MDPI, Basel, Switzerland. This article is an open access article distributed under the terms and conditions of the Creative Commons Attribution (CC BY) license (https://creativecommons.org/licenses/by/4.0/).

1. Introduction

Bauxite residue (BR), also known as "red mud", is the main residue of the alumina industry. It is generated as a slurry through the high-pressure leaching of bauxite with sodium hydroxide in the Bayer process [1]. Its chemical and mineralogical composition is complex and variable, depending on the geochemistry of the original bauxite ore. Typically, BR contains iron (Fe^{3+}) oxides (30–60 wt.%), aluminum hydroxides (10–20 wt.%), titanium oxides (from trace amounts up to 25 wt.%), and various sodium–aluminum silicate phases (up to 20 wt.%). The latter phases are formed secondarily during the reaction of the bauxite mineral phases with the NaOH. Bauxite residue poses a significant environmental hazard due to the following: (a) its high alkalinity (pH ranging from 10 to 13), (b) its fine colloidal particle size distribution (including submicron and nano-scale particles), (c) the presence of

various trace heavy metals and metalloids, and (d) the occurrence of naturally occurring radioactive materials (NORMs) such as ^{238}U, ^{226}Ra, ^{232}Th, and ^{40}K [1–3]. It is estimated that about 180 million tons of BR are produced annually, while 4 billion tons have been already accumulated on a global scale [4], rendering it one of the most hazardous residues of the metallurgy industry. This situation is expected to worsen, given that global aluminum demand is projected to increase by nearly 40% by 2030 [5].

Wet disposal (lagooning) of BR, which is still practiced at several alumina plants worldwide [6–8], can simultaneously have serious impacts on ecosystems (including surrounding soils and groundwater), human health, and associated natural resources. Evaporation ponds used in this method are vulnerable to natural disasters, and have led to major accidents in the past, such as the Ajka spill in Hungary in 2010 and the Luoyang incident in China in 2016 [9,10]. Currently, the most widely adopted BR management technique is dry disposal, which involves the filter-pressing of the residue prior to its disposal. While this method reduces certain environmental risks originated by the slurry-like form of the residue, it comes with high operational costs and does not entirely eliminate environmental concerns.

During the last decades, much research has focused on BR valorization aiming either to produce high-value-added materials or to extract various metals. Following the first approach, BR has been used in the synthesis of bricks [11], glass ceramics [12], cement [13], geopolymer materials [14] and subgrade materials [15], among others. On the other hand, BR is considered a secondary resource of various metallic values including iron, aluminum, titanium, gallium, and rare earth elements, and while respective metallurgical methodologies have been applied, only a limited number of them have been scaled up to the pilot or semi-industrial scale for the extraction of these metals [16]. Iron recovery has attracted the greatest interest as, in several cases, it is a necessary step for the co-extraction of other valuable metals. Investigated pyro-metallurgical techniques include the following: (a) the magnetic separation of the untreated residue via successive separation steps [17], (b) the low-temperature roasting of BR, aiming to form magnetite, followed by magnetic separation [18,19] and high-temperature reductive smelting [20,21]. A number of studies involve the use of alternative heating sources such as microwaves [22,23], green reducing agents [24,25], and alkaline salt additives that enhance iron recovery [26]. Despite the applicability of these techniques to iron recovery, they present important drawbacks such as the following: low recovery yields, high energy consumption, and complexity. The hydrometallurgical reduction of red mud is proposed as an alternative promising methodology. It is based on the transformation of the initial hematite phase to magnetite under high pressure alkaline conditions [26–29]. The resulting iron-rich secondary residue can be directly further processed via wet magnetic separation, while the aluminum-rich liquor can be reintroduced into the Bayer circuit. Although this method has so far only been applied at a small scale, it offers several advantages, including the following: (a) lower electrical energy consumption compared to pyro-metallurgical reductive roasting or smelting, and (b) a more holistic residue management strategy, as the largest portion of the BR can potentially be recycled.

The present article focuses on BR samples sourced from alumina refineries in Konya, Turkey (ETI Seydişehir Alüminyum S.A.) and Tulcea, Romania (VIMETCO), which, along with a Greek refinery in Agios Nikolaos, Greece (METLEN), participated in the REEScue project (https://reescue.com, accessed on 10 September 2025). This specific project is included within the framework of the European research network ERA-MIN2, which focus-es on the processing of raw materials through innovative technologies (https://www.era-min.eu accessed on 10 September 2025). The study investigates the magnetic separation behavior of these two low-iron-grade secondary residues following hydrothermal reduction, which

aims to convert hematite to magnetite and enhance the magnetic susceptibility of the iron-bearing phases. Separation efficiency was evaluated in terms of iron grade and recovery. In certain tests, sonication of the slurry was applied to inhibit particle agglomeration. The results were compared with those obtained from the magnetic separation of the untreated bauxite residues.

2. Materials and Methods

2.1. Bauxite Residue Materials

The BR samples used in this study were collected from the Eti Alüminyum plant in the Seydişehir district of Turkey and the Alum plant in Tulcea, Romania. In both cases, sampling was conducted using an excavator to obtain approximately 0.5–1 tons of material, which was subsequently homogenized with a compact track loader. Sample reduction was performed using the mixing and quartering method.

2.2. Analytical Techniques

The bulk chemical analysis of the collected and hydrothermally reduced residue materials was performed via X-ray fluorescence spectrometry (XRF) using a SPECTRO XEPOS ED-XRF spectrometer (SPECTRO Analytical Instruments, Kleve, Germany). Prior to the analysis, the samples were vitrified using a flux mixture of Li-tetraborate and Li-metaborate flux at a mass ratio 1:1 and 1% LiBr as a binding agent. The mineralogical analysis of the initial and reduced samples was conducted through X-ray diffractometry using a using a Bruker D8 Focus diffractometer (Bruker, Billerica, MA, USA) equipped with a Cu-Kα (Ni-filtered) radiation source, scanning from 5° to 75° in the 2θ range at a step size of 0.02° per second. Reduced BR samples were morphologically investigated with scanning electron microscopy using a JEOL6380LV SEM/EDS (JEOL Ltd. Tokyo, Japan) system operating at 20 kV, with a probe current of 1.5 nA. The semi-quantitative mineralogical analysis of the initial and reduced samples was performed via Rietveld methodology using the Profex 4.3.1 software [30]. Details on the implementation of Rietveld methodology for the identification of mineral phases in BR and hydrothermally reduced BR samples are given elsewhere [29].

2.3. Hydrothermal Reduction

The hydrothermal alkaline reduction of bauxite residue primarily targets the transformation of hematite (Fe_2O_3) and goethite [FeO(OH)] into magnetite (Fe_3O_4) in order to increase the magnetic susceptibility of the material and enhance its magnetic separation. The process has been optimized within the framework of a previous study [29] and the optimum conditions are presented in Table 1. Hydrothermal treatment was carried out in a 600 mL Parr autoclave reactor (4842 series) (Parr, Moline, IL, USA) constructed from Inconel 625 alloy, able to withstand high alkaline environments at elevated temperatures (up to 300 °C). The magnetite phase is contained in the precipitate separated via filtration, while the largest portion of the initial aluminum amount contained in the aluminum hydroxide phases is dissolved and transferred to the liquor. In addition to sodium hydroxide, a quantity of iron(II) sulfate hydrate is added as a source of ferrous ions, which enhances the reduction of the hematite and goethite in the residue to magnetite. Furthermore, $FeSO_4 \cdot 7H_2O$ leads to the generation of $Fe(OH)_3^-$ which reacts with the titanium phases, forming titanium–iron compounds. As a result, the formation of a superficial sodium titanate coating—commonly observed on aluminum hydroxide particles—is prevented,

thereby improving aluminum in the liquor [17]. The conversion of hematite (or goethite) to magnetite is calculated as follows:

$$\eta(Fe_2O_3 \text{ or } \alpha\text{–FeOOH})\% = 100\% \cdot [1 - m_{res}Fe(III)/m_{BR}Fe_{tot}] \quad (1)$$

Here, $m_{res}Fe(III)$ represents the mass of Fe(III) in the hematite or goethite that remains in the residue after hydrochemical processing, while $m_{BR}Fe_{tot}$ is the total mass of iron present in the original bauxite residue sample.

Table 1. Experimental parameters followed for the hydrothermal processing of bauxite residue.

Parameter	Value
Operating Temperature	250 °C
Agitation Speed	400 rpm
Pressure	500 psi
Leaching Agent	NaOH (5 M)
Pulp Density	20%
$FeSO_4 \cdot 7H_2O$	Fe^{2+}/Fe_{tot} ratio: 0.3
Reaction Time	3 h

2.4. Wet Magnetic Separation

Wet magnetic separation was employed to obtain an iron-rich magnetic fraction from both the raw BR samples and the hydrothermally reduced samples. The reduced residue, in slurry form, was fed directly into the magnetic separator. The separation tests were conducted using a Carpco MWL-3465 lab-scale high-intensity magnetic separator (OUTOKUMPU TECHNOLOGY, INC., Wildwood, FL, USA), while the slurry was prepared using a Heidolph stirrer (Heidolph Instruments GmbH & Co. KG, Schwabach, Germany) set at 2000 rpm. The magnetic field intensity was measured using an AC/DC magnetic meter (model MF100, Extech Instruments, Nashua, NH, USA). The applied experimental conditions are displayed in Table 2. Preliminary tests indicated minor changes to the recovery at magnetic induction over 2000 Gs; therefore, magnetic fields with lower intensity levels were applied. The improvement of the particle dispersion, by the avoidance of agglomeration phenomena, was examined by the combination of mechanical stirring and the application of ultrasound. The ultrasonic homogenizer UP200S (Hielscher Ultrasonics GmbH, Teltow, Germany) was used for the formation of pulses.

Table 2. Experimental parameters used for the magnetic separation of untreated and hydrothermally processed bauxite residue.

Parameter	Value
Magnetic Induction	70–1600 Gs (7×10^{-3}–1.6×10^{-1} T)
Slurry Concentration	2 wt.%
Fluid Flow Rate	0.1 L/min
Ultrasound Amplitude	75% (0.75 s ON, 0.25 s OFF)

3. Results

3.1. Physicochemical Characterization of the Bauxite Residue Samples

The bulk chemical and mineralogical analyses of the initial bauxite residues (Romania—RBR; Turkey—TBR) are presented in Table 3 and Figure 1, respectively. The iron oxide content ranges from approximately 35 to 40 wt.%, with a higher concentration in the RBR sample. Both samples can be classified as low-iron-grade samples, according to the literature, where bauxite residues with Fe_{elem} contents exceeding 47 wt.% have been reported [18]. The

residual aluminum hydroxide content, expressed as Al_2O_3, is similar in both samples, at around 17 wt.%. X-ray diffraction patterns reveal that the iron oxide phase in TBR is exclusively hematite, whereas in RBR it exists as a mixture of hematite and goethite. With respect to the aluminum hydroxide contents, only the gibbsite phase is detected for RBR, while TBR contains both gibbsite and boehmite. Regarding the secondary phases formed during the Bayer process, an intense sodalite peak is observed in both materials. Additionally, cancrinite and a mica-group species (potentially paragonite) are identified in the TBR sample (Figure 1). At this point, it should be noted that the intensity of the mica phase is close to the detection limit of the XRD-Rietveld method, and the precise identification of the specific mica-group species is challenging due to the mineralogical complexity of the samples. The mineralogical composition of the residues was quantitatively estimated according to the Rietveld methodology, and the results are presented in Table 4. Before this, the amorphous content in both samples was determined, and found to be below 5% in both samples. The hematite/goethite mass ratio in RBR is approximately 3:1. Both samples contain a significant amount of calcite, while RBR is richer in silica phases, such as quartz and tridymite. Titanium exists as rutile in both residues.

Table 3. Chemical analysis of the initial bauxite residue samples.

Components	RBR	TBR
Fe_2O_3	39.2	35.3
(Fe_{elem})	27.4	24.7
Al_2O_3	17.4	17.9
SiO_2	11.5	14.7
Na_2O	6.7	7.0
CaO	4.9	4.9
TiO_2	2.2	4.2
LOI	16.3	14.1
Other	1.8	1.9

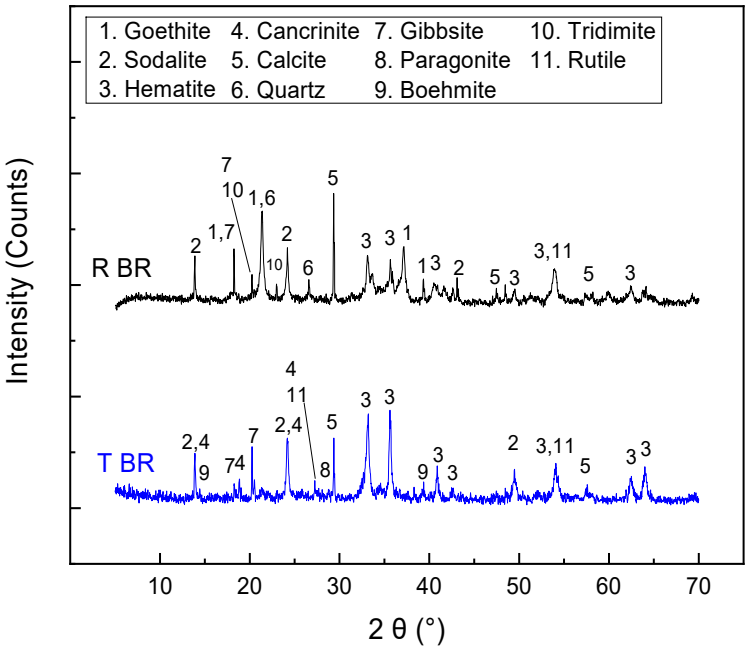


Figure 1. X-ray diffraction patterns of the initial bauxite residues (RBR and TBR).

Table 4. Mineralogical composition (wt.%) of the bauxite residues.

Mineral Species	Chemical Formula	Content (wt.%)	
		RBR	TBR
Al-Goethite	$Al_{0.1}Fe_{0.9}OH$	44.3	0.0
Sodalite	$Al_6Na_6Si_6C_{2.4}O_{34.32}H_{23.04}$	17.1	18.2
Hematite	Fe_2O_3	13.3	43.1
Cancrinite	$Al_6Na_{7.14}Si_{7.08}O_{31.6}H_{9.74}$	0.0	11.4
Calcite	$CaCO_3$	10.3	7.6
Quartz	SiO_2	3.2	0.0
Gibbsite	$Al(OH)_3$	3.1	6.7
Mica-group	$Al_3NaSi_3O_{12}H_2$	0.0	3.4
Boehmite	AlO(OH)	0.0	1.0
Ca-Na-Al oxide	$Al_6Ca_{8.25}Na_{1.5}O_{18}$	0.0	0.9
Tridymite	SiO_2	2.6	0.0
Cristobalite-α	SiO_2	0.0	0.8
Rutile	TiO_2	1.8	3.5
Amorphous		4.3	3.6

The microstructure of the RBR and TBR samples was revealed through scanning electron microscopy. The RBR samples display an inhomogeneous particle size distribution, ranging from a few μm to up to 200 μm. Iron (Fe^{3+}) oxides in few cases occur as relative pure particles, and mostly co-exist with aluminum oxyhydroxide in agglomerated particles (Figure 2a,b). Small particles rich in Ca-Na-Al-Si form a colloidal substrate. Iron–titanium-rich particles (i.e., titanomagnetite or/and ilmenite) occur as relatively large (up to 100 μm), angular particles. Isolated silicate–zircon particles are rarely identified.

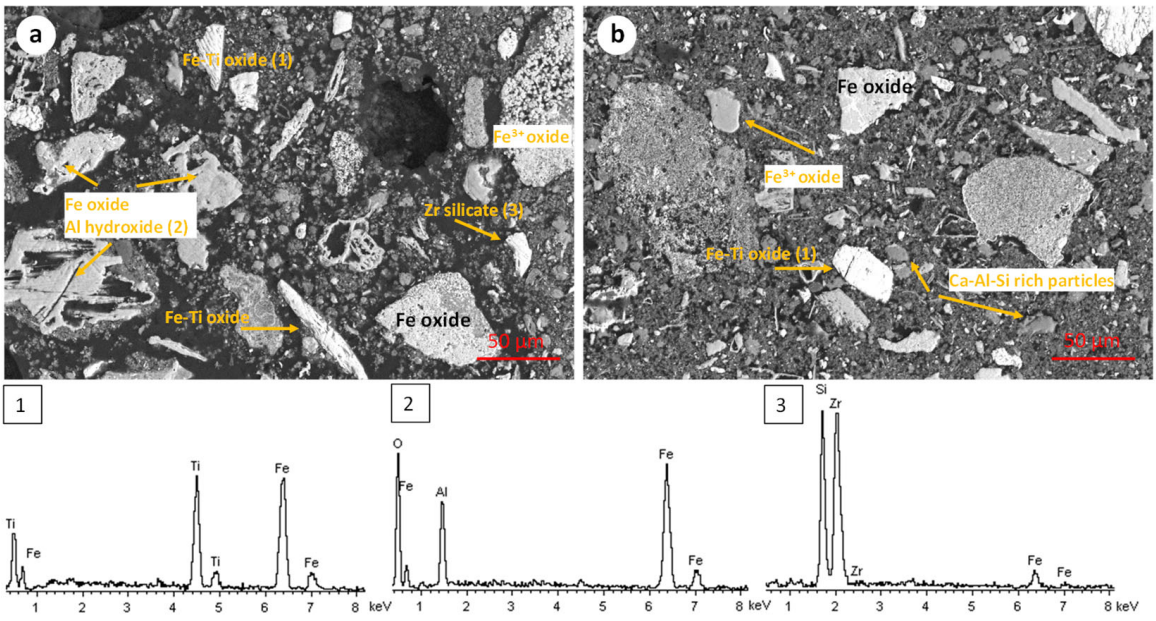


Figure 2. Scanning electron micrographs and corresponding representative EDS spectra of the initial RBR sample. The EDS spectra are numbered according to the phases shown in the SEM micrographs.

The TBR sample presents a similar microstructure and microchemical characteristics (Figure 3). Iron oxide (Fe^{3+}) exists either as relatively pure particles (up to 100 μm) or, most commonly, as intergrowths of iron oxide-iron hydroxide (Figure 3a). Relatively large agglomerated particles with more than one chemically distinctive region (iron oxide or iron–titanium oxide, aluminum hydroxide, and Ca-Fe-Al-Si) were observed (Figure 3b). The overall scanning electron microscopy investigation of both the RBR and TBR sam-

ples indicates the chemical complexity and the agglomerated structure of the materials, rendering the isolation of the iron oxide fraction, through magnetic separation, unlikely.

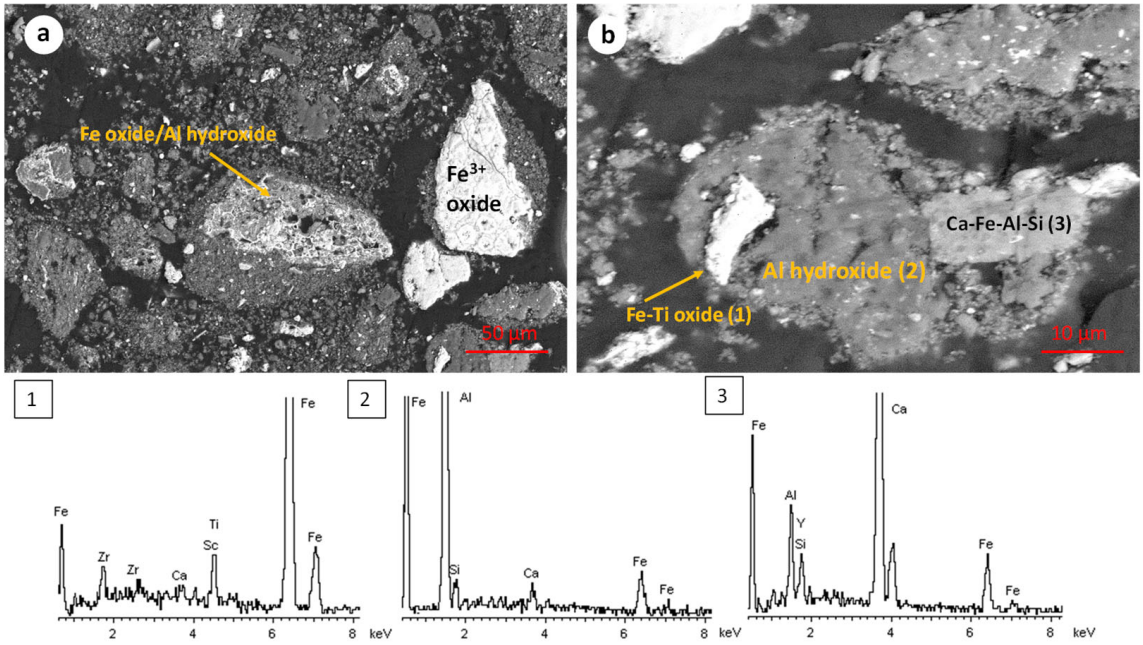


Figure 3. Scanning electron micrographs and corresponding representative EDS spectra of the initial TBR sample. The EDS spectra are numbered according to the phases shown in the SEM micrographs.

3.2. Alkaline Hydrothermal Reduction

The hydrothermal reduction treatment step aims to produce transformed residue with an increased Fe_{tot} content and a dominant magnetite phase, which will be readily submitted to a subsequent wet magnetic separation. The transformation of hematite to magnetite is well established from both a thermodynamic and mechanistic perspective [28,29,31], and it is based on the reaction of the Fe_2O_3 with the metastable ferrous ion species $FeOH^+$ and $HFeO_2^-$, all of which are formed upon the addition of ferrous sulfate into the autoclave. After the reduction process, the Fe_{tot} content in both samples increases, primarily due to the addition of the iron sulfate reagent and the transfer of a significant amount of aluminum into the liquor (Tables 3 and 5).

Table 5. Chemical analysis of the hydrothermally reduced bauxite residue samples.

Components	Treated RBR	Treated TBR
Fe_2O_3	59.3	43.7
(Fe_{elem})	41.5	30.6
Al_2O_3	9.4	11.6
SiO_2	12.7	15.5
Na_2O	4.9	8.4
CaO	5.4	6.8
TiO_2	3.0	5.0
LOI	2.7	6.2
Other	2.6	2.8

X-ray diffractometry accompanied by Rietveld quantitative analyses (Figure 4, Table 6) showed that hematite and goethite phases in RBR and TBR are partially reduced to magnetite. The conversion degree of Fe^{3+} oxides to magnetite reaches 76% in the case of RBR, and 49.6% in the case of TBR. Cancrinite is the major non-ferrous species in both reduced

residues. The sodalite content in both samples is significantly reduced compared to the initial samples. Gibbsite concentrations remain largely unchanged, with a slight decrease observed in RBR and a slight increase in TBR. Boehmite is not detectable, indicating the leaching of aluminum in the alkaline liquor (Table 4). The presence of non-dissolved gibbsite may be attributed to its encapsulation in refractory phases. The calcite amount is significantly reduced; however, calcium-containing phases were not detected in the reduced samples via X-ray diffractometry. According to the literature, calcium carbonate is converted to $Ca(OH)_2$ in the presence of NaOH [32], suggesting that $Ca(OH)_2$ may have formed as an amorphous phase. On the contrary, reduced samples are enriched in rutile. The limited reducibility of the TBR sample can be attributed to specific structural characteristics, not revealed through SEM investigation, which possibly enhance agglomeration phenomena and impede the reduction reaction.

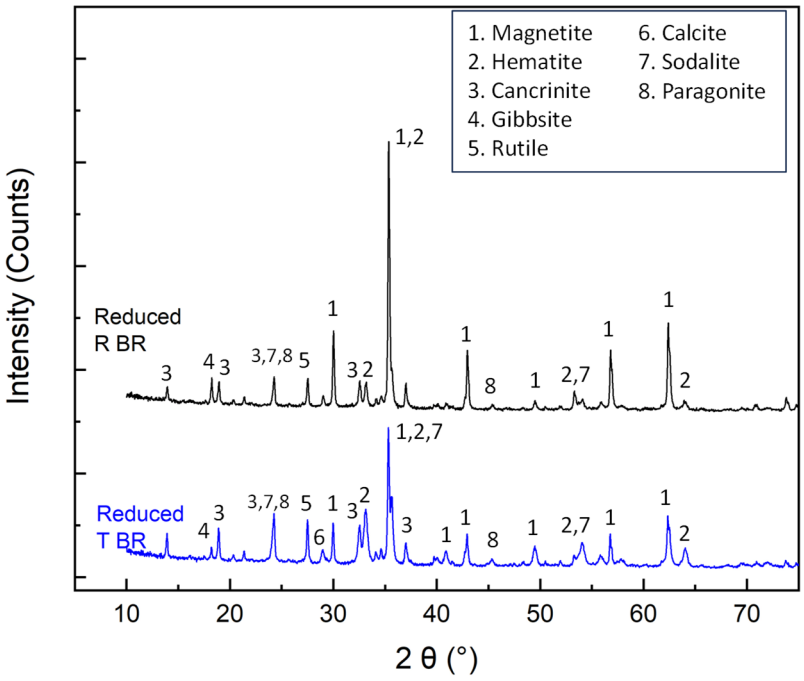


Figure 4. X-ray diffraction patterns of the hydrothermally reduced RBR and TBR samples.

Table 6. Mineralogical composition (wt.%) of the bauxite residue samples after their hydrothermal reduction.

Mineral Species	Chemical Formula	Content (wt.%)	
		RBR	TBR
Magnetite	Fe_3O_4	47.3	27.9
Sodalite	$Al_6Na_6Si_6C_{2.4}O_{34.32}H_{23.04}$	3.0	7.6
Hematite	Fe_2O_3	9.8	19.1
Cancrinite	$Al_6Na_{7.14}Si_{7.08}O_{31.6}H_{9.74}$	19.4	23.7
Calcite	$CaCO_3$	2.3	2.0
Gibbsite	$Al(OH)_3$	5.3	5.2
Mica group (potentially paragonite)	$Al_3NaSi_3O_{12}H_2$	2.4	3.5
Rutile	TiO_2	2.8	4.6
Other		1.3	1.1
Amorphous		6.3	5.3
Conversion degree to magnetite η(Fe_2O_3 or α–FeOOH)%		76.7	49.6

The microstructure of the hydrothermally reduced RBR and TBR samples is shown in the SEM micrographs in Figure 5. The presence of iron oxide and Ti-containing iron oxide particles is observed. EDS semi-quantitative analysis indicates that the iron-to-oxygen mass ratio in both phases corresponds to that of magnetite. The titanium concentration in the Ti-containing particles (titanomagnetite or/and ilmenite) is up to 5 wt.%. These particles likely consist of a mixture of Fe_3O_4 and titanium dioxide, or they may correspond to titanomagnetite species. Their precise mineralogical micro-composition will be investigated, using transmission electron microscopy, in a future work. In several cases, magnetite particles (Figure 5a–d) exhibit a hollow structure, which may be attributed to a dissolution–reprecipitation mechanism during the transformation of Fe^{3+} oxides into the magnetite phase. This specific mechanism has been reported in aqueous systems containing iron oxides [33,34].

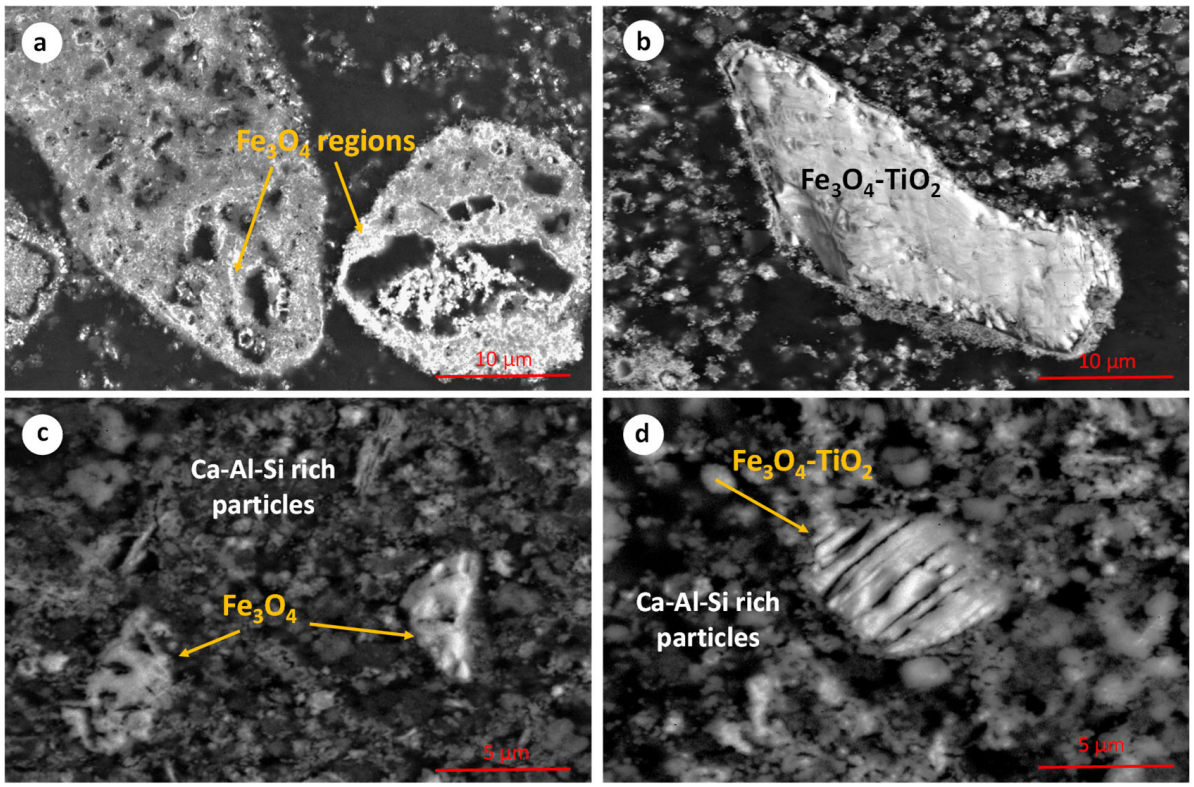


Figure 5. Scanning electron micrographs of the hydrothermally reduced RBR (**a**,**b**) and TBR (**c**,**d**) samples.

3.3. Magnetic Separation Tests

This part of the study focuses on optimizing the wet magnetic separation process of the RBR and TBR samples, to obtain an iron-enriched and partially reduced concentrate. To achieve this, two series of tests were conducted: one involving the magnetic separation/iron enrichment of the initial untreated bauxite residue samples, and the other involving the magnetic separation of the respective hydrothermally reduced samples. A magnetic induction in the range of 5–1600 Gs was selected for the untreated samples and a range of 5–700 Gs for the more magnetically susceptible reduced samples. The dispersion of the reduced BR sludge in the magnetic separator was achieved either through agitation alone or through a combination of agitation and ultrasound application. Given the extent of the experimental data presented in this section, a more comprehensive discussion of the results and the interplay among the various material and process parameters is provided separately in Section 3.4 (Separation performance).

Figure 6 illustrates the mass distribution of magnetic and non-magnetic fractions resulting from the magnetic separation of both the untreated (Figure 6a,c) and the hydrothermally reduced RBR samples (Figure 6b,d), which were dispersed either through agitation or combining agitation and sonication. Low retention is observed in the case of the untreated RBR sample—particularly when magnetic induction values up to 700 Gs are applied. Under these conditions, the magnetic fraction does not exceed 41.6% of the initial feed mass, indicating low iron oxide retention (the initial iron oxide content in the sample was 39.18 wt.%—see Table 3). Increasing the magnetic induction to 1600 Gs significantly improves retention (Figure 6a). When ultrasound is applied, a consistent reduction of 10–15% in the magnetic fraction is observed across the entire range of magnetic induction (Figure 6c), suggesting that this method of dispersion hinders magnetic agglomeration or alters dispersion behavior.

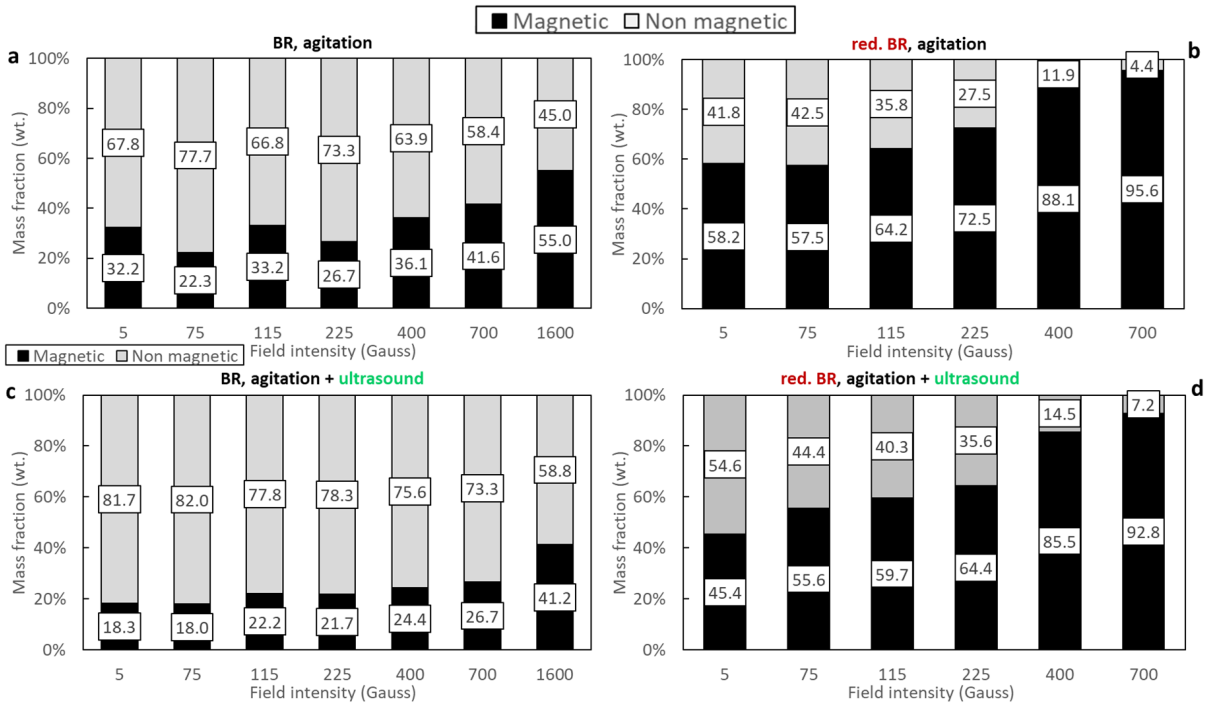


Figure 6. Magnetic and non-magnetic mass fractions as a function of the magnetic field of the: untreated RBR using agitation (**a**), untreated RBR using agitation/ultrasonication (**c**), reduced RBR using agitation (**b**), and reduced RBR using agitation/sonification (**d**).

The results of the hydrothermally treated samples differ considerably, mainly in terms of the mass fraction of the magnetic sample (Figure 6b,d). In this case, most of the feed is retained in the magnetic fraction even at very low magnetic induction values (5 Gs), indicating a significant enhancement in magnetic susceptibility. Notably, the use of ultrasound together with agitation results in a lower magnetic mass fraction compared to agitation alone, with the most pronounced reduction observed at the lowest magnetic induction (5 Gs), where a 12.8% decrease is recorded.

Figure 7 illustrates the magnetic separation results for the untreated and hydrothermally treated TBR samples. Poor magnetic retention is observed during the processing of the untreated TBR sample (Figure 7a,c). When only agitation is applied, the mass of the magnetic fraction remains below 34.5% across the entire range of magnetic induction (0.1–1600 Gs). Similar to the Romanian sample, the combination of agitation with ultrasound leads to a 10–15% reduction in magnetic fraction recovery (Figure 7c). Following hydrothermal treatment, the TBR sample demonstrates a significant improvement in magnetic separation performance. The magnetic fraction progressively increases with increasing

magnetic induction, reaching nearly 91% at 700 Gs (Figure 7b). However, the application of both agitation and ultrasound again results in a reduction in the magnetic fraction, with the effect being more pronounced at lower magnetic induction values (<225 Gs), suggesting that ultrasound-assisted dispersion reduces particle aggregation or magnetic bridging during separation (Figure 7d).

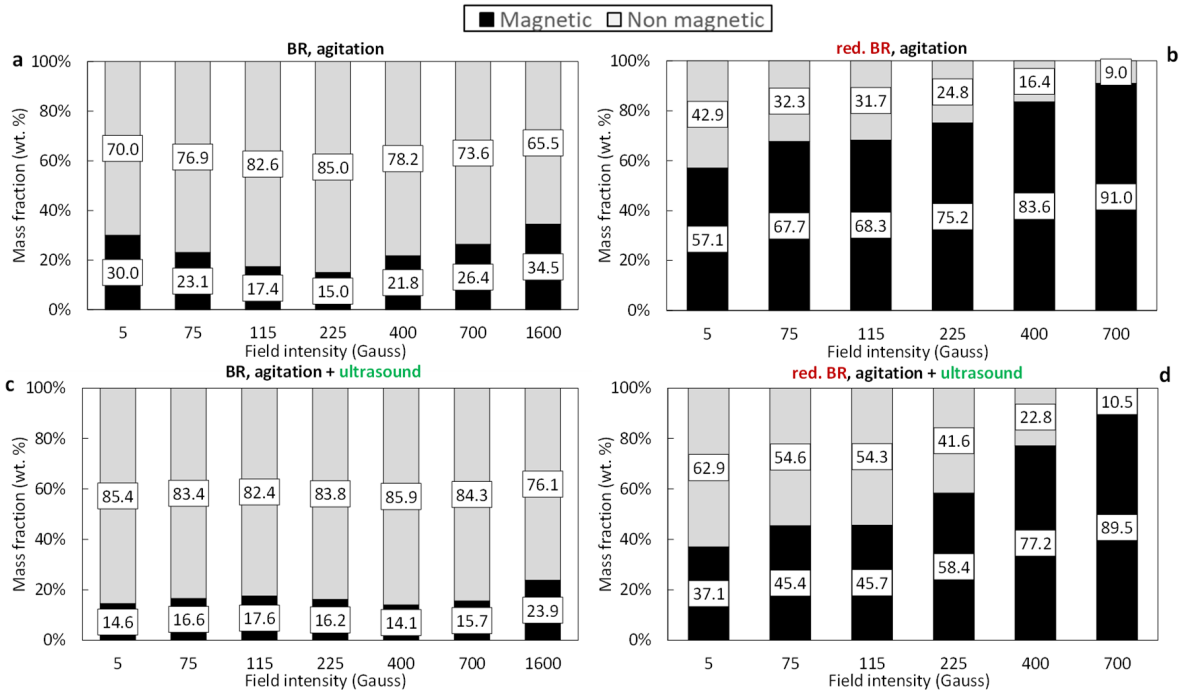


Figure 7. Magnetic and non-magnetic mass fractions as a function of the magnetic field of the: untreated TBR using agitation (**a**), untreated TBR using agitation/ultrasonication (**c**), reduced TBR using agitation (**b**), and reduced TBR using agitation/sonification (**d**).

Comparing the results, it appears that higher magnetic fractions are obtained from the RBR sample (raw or treated) relative to the TBR one. This result can be attributed to the elevated iron concentrations in RBR. Untreated RBR has a slightly higher Fe (Fe_2O_3 = 39.2%) compared to the Turkish one (Fe_2O_3 = 35.2%), while reduced RBR has significantly higher iron content (Fe_2O_3 = 59.3%) in comparison to the TBR sample ($F_{e2}O_3$ = 43.7%).

The iron oxide (Fe_2O_3 and/or Fe_3O_4) recovery and grade in the magnetic fractions obtained from the RBR and TBR samples under various conditions are presented in Figures 8a–d and 9a–d, respectively. Magnetic fractions obtained from the untreated RBR sample show relatively low elemental iron concentrations, around 30 wt.%, corresponding to approximately 42.8 wt.% hematite—only slightly higher than the initial residue concentration. Simultaneously, a significant portion of iron—up to 66.2 wt.% at 5 Gs—is lost in the non-magnetic fraction (Figure 8a). The application of ultrasound negatively impacts both the iron grade in the magnetic fraction and the iron recovery (Figure 8c); the Fe recovery decreases by 20.1% during separation at 1600 G when agitation and sonication are combined (39.6%), compared to just agitation (59.7%).

The reduced RBR sample exhibits much better magnetic separation selectivity for iron. In this case, elemental iron concentrations in the magnetic fraction increase to approximately 45 wt.%, and iron recovery is as high as 98%. Also, the application of ultrasounds adversely affects Fe recovery (Figure 8d).

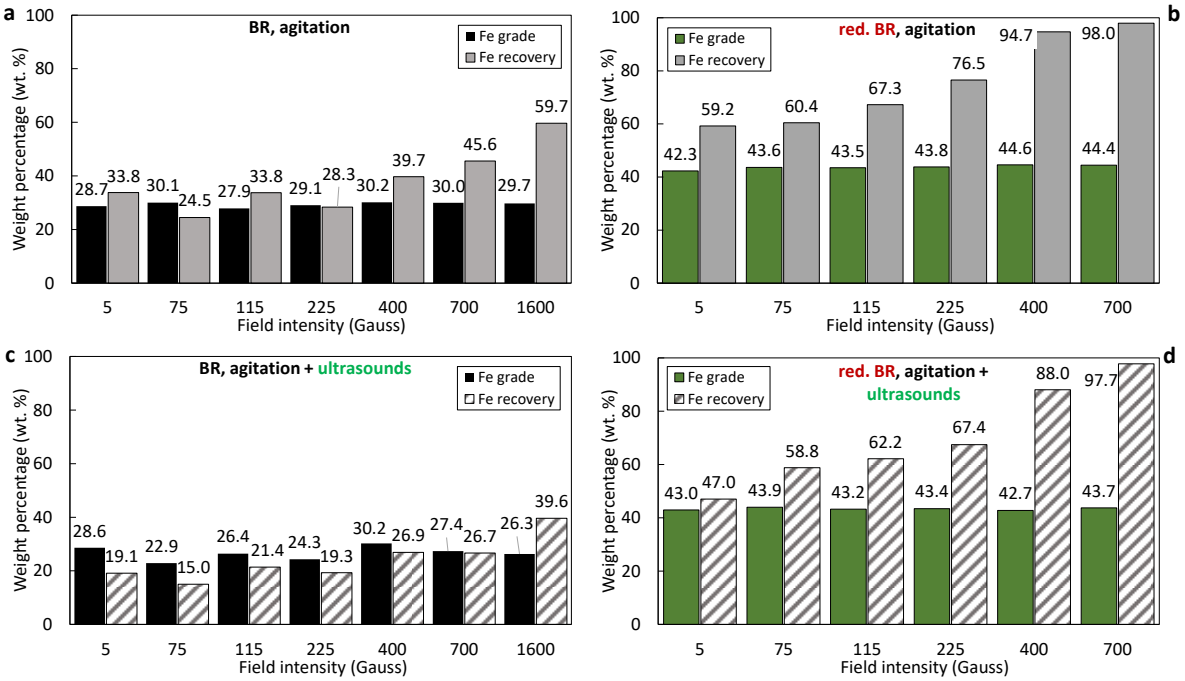


Figure 8. Iron recovery and grade (%) as a function of the magnetic induction in magnetic fractions produced by the separation of the: untreated RBR under agitation (**a**), untreated RBR under the combination of agitation and sonication (**c**), reduced RBR under agitation (**b**), and reduced RBR under the com-bination of agitation and sonication (**d**).

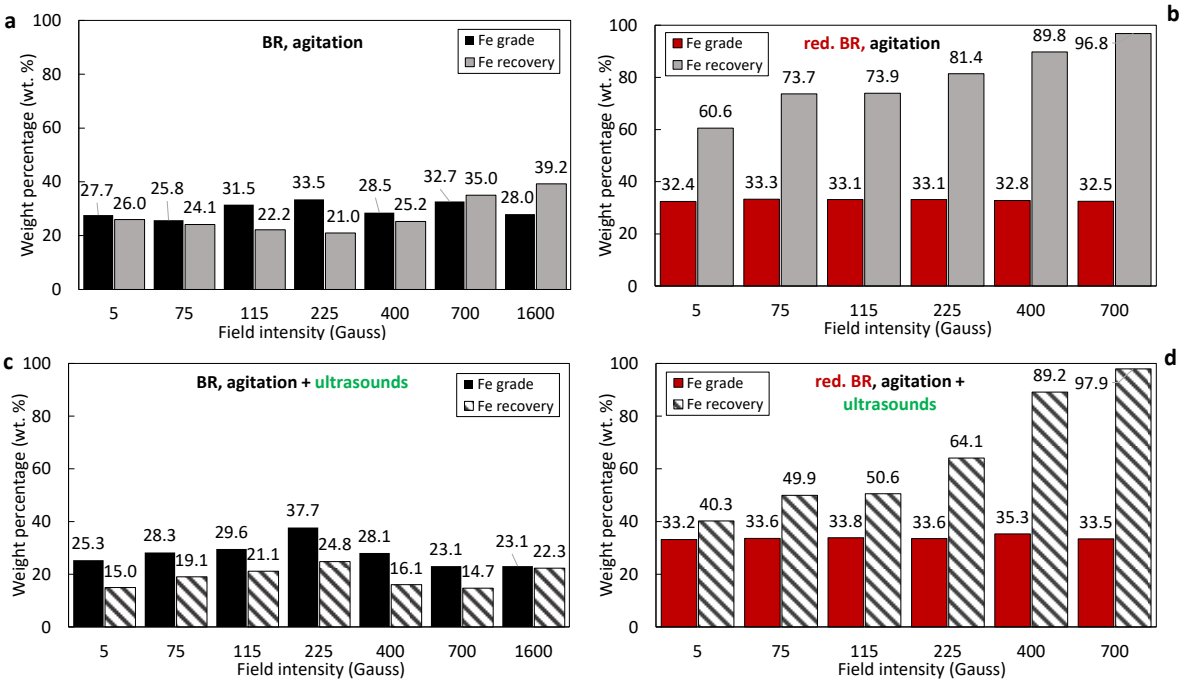


Figure 9. Iron recovery and grade (%) as a function of the magnetic induction in magnetic fractions produced by the separation of the: untreated TBR under agitation (**a**), untreated TBR under the combination of agitation and sonication (**c**), reduced TBR under agitation (**b**), and reduced TBR under the combination of agitation and sonication (**d**).

Similar trends were observed for the TBR sample (Figure 9a–d). In all cases—whether using untreated or treated samples, with or without ultrasound—the iron grade in the magnetic fractions and the iron recovery are consistently lower than those for the RBR sample. This reflects the lower initial iron content of the TBR material, as well the lower

conversion degree to magnetite. RBR shows higher magnetic separation efficiency in terms of Fe grade in the magnetic concentrate, compared to the TBR sample. In general, the achieved iron grade and recovery under optimum conditions in both the reduced RBR and TBR samples (magnetic induction of 700 Gs and slurry dispersion through agitation) are generally comparable to those obtained from magnetic fractions produced by the separation of bauxite residues roasted under mild conditions according to the relative literature [18,19].

Figure 10a–d presents the distribution of selected oxides (Na_2O, Al_2O_3, SiO_2, CaO, TiO_2) in the magnetic fraction as a function of the magnetic induction applied during the separation, for both the untreated and the hydrothermally reduced RBR. If the distribution of an oxide in the magnetic fraction exceeds the mass yield, then enrichment of the magnetic concentrate in the specific oxide occurs.

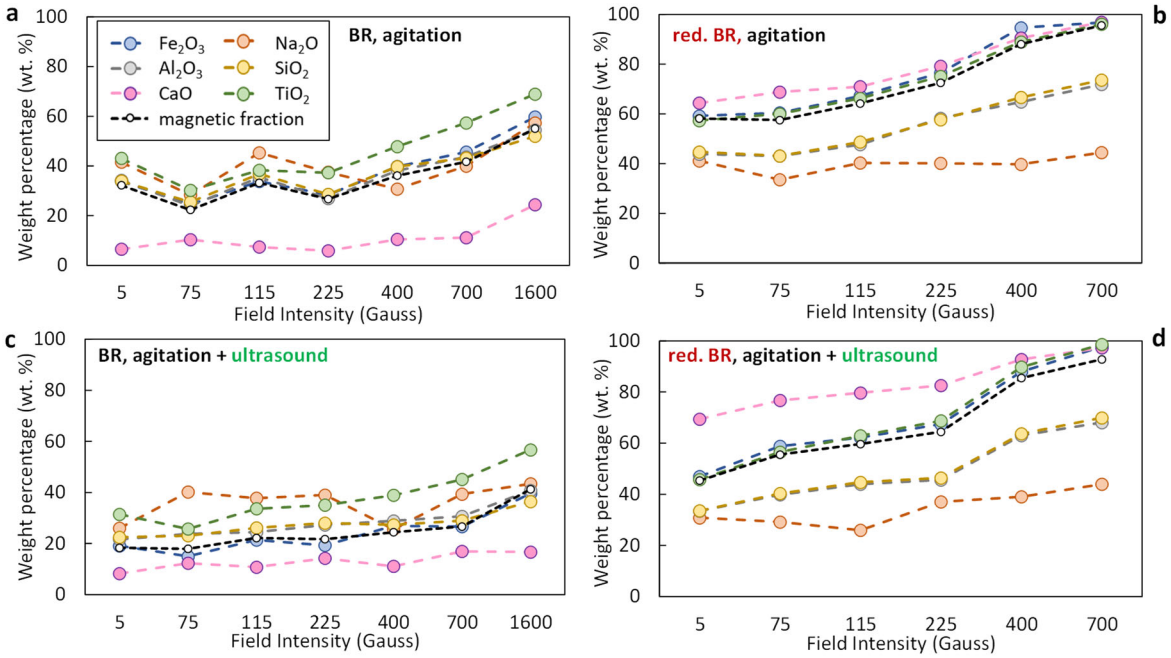


Figure 10. Distribution of major oxides (Fe_2O_3, Al_2O_3, Na_2O, SiO_2, CaO, TiO_2) in the magnetic fraction obtained from Romanian-origin bauxite residue (BR) (**a**,**c**) and hydrothermally reduced bauxite residue (red. BR) (**b**,**d**), as a function of the applied magnetic induction. The black dashed line indicates the weight percentage of the magnetic fraction relative to the feed. Particle dispersion occurred either through agitation (**a**,**b**) or by combining agitation and ultrasounds (**c**,**d**).

In the untreated BR, iron shows increasing transfer to the magnetic fraction as magnetic induction increases (Figure 10a); with simple agitation, approx. 40% of the Fe_2O_3 is transferred to the magnetic fraction at 400 Gs, rising to approx. 60% at maximum magnetic induction (1600 Gs), with the mass yield increasing from approx. 35% to 55% over that range. Upon combining agitation with ultrasound (Figure 10c), Fe_2O_3 transfer reduces, reaching almost 18% at 5 Gs with a similar magnetic yield value, indicating poor separation efficiency. Slightly increased distributions of the major gangue components Al_2O_3 and SiO_2, regardless of the dispersion method, indicate poor selectivity of the separation. CaO is an exception, presenting lower distribution in the magnetic fraction, which is considerably reduced in the agitation-only case, being below 10% for separation by magnetic induction below 1600 Gs.

In the treated sample (Figure 10b,d), a significant enhancement in iron recovery is observed, due to the transformation of hematite into magnetite during the hydrothermal reduction process. At 400 Gs, approximately 90% of the Fe_2O_3 is recovered in the magnetic fraction (Figure 10b), increasing to around 95% at 700 Gs. Similar values are maintained

across the range of applied magnetic field intensities, confirming the improved magnetic response of the reduced material. When ultrasound is applied in combination with agitation (Figure 10d), both Fe_2O_3 distribution and magnetic mass yield are maximized, reaching approximately 98% and 95%, respectively, at 700 Gs. Despite this high iron recovery, the distribution of Al_2O_3 and SiO_2 in the magnetic fraction remains at around 65%, indicating moderate selectivity. It is also noteworthy that the magnetic fraction consistently shows reduced inclusion of Al_2O_3 and SiO_2 across the entire magnetic induction range, reflecting partial separation of these gangue oxides from the iron-rich phases. Even more selective behavior is observed for Na_2O, whose distribution in the magnetic fraction remains considerably lower throughout, further highlighting the improved separation efficiency achieved after reduction, particularly in combination with ultrasound-assisted dispersion.

The distribution of selected oxides (Na_2O, Al_2O_3, SiO_2, CaO, TiO_2) in the magnetic fraction as a function of the applied magnetic induction during separation for both the untreated and hydrothermally reduced TBR is shown in Figure 11. In the case of the untreated BR, under agitation alone (Figure 11a), magnetic separation is relatively inefficient. The recovery of Fe_2O_3 to the magnetic fraction ranges from approximately 18% at 225 Gs to around 50% and 40% at 5 and 1600 Gs, respectively. The magnetic fraction yield varies between 15% and 30% across the field range, with the lowest value (~15%) observed at 225 Gs. Notably, significant portions of non-ferrous oxides—such as Al_2O_3 and SiO_2—are also recovered in the magnetic product, indicating poor selectivity. Similar results are obtained when agitation is combined with ultrasound (Figure 11c), suggesting that TBR exhibits a limited response to dispersion enhancement alone. Unlike the RBR sample, the TBR sample shows overall lower magnetic separation performance, likely due to its lower inherent magnetic susceptibility and weaker dispersion response.

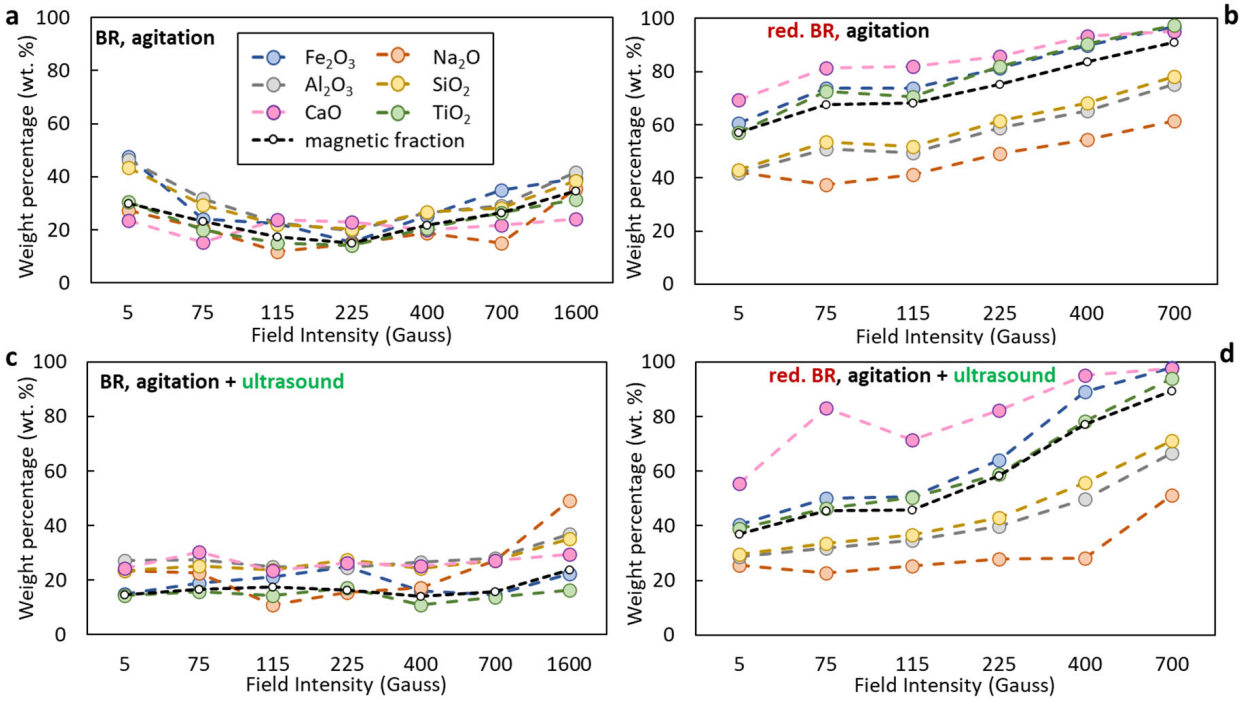


Figure 11. Distribution of major oxides (Fe_2O_3, Al_2O_3, Na_2O, SiO_2, CaO, TiO_2) in the magnetic fraction obtained from Turkish-origin bauxite residue (BR) (**a**,**c**) and hydrothermally reduced bauxite residue (red. BR) (**b**,**d**), as a function of applied magnetic induction. The black dashed line indicates the weight percentage of the magnetic fraction relative to the feed. Particle dispersion occurred either through agitation (**a**,**b**) or by combining agitation and ultrasounds (**c**,**d**).

Hydrothermal treatment substantially improves magnetic separation performance. Both the mass yield of the magnetic fraction and the distribution of Fe_2O_3 increase markedly across the entire magnetic induction range compared to the untreated sample. As shown in Figure 11b, the magnetic yield increases from ~55% at 5 Gs to nearly 90% at 700 Gs, while Fe_2O_3 recovery rises from ~55% to almost 98% within the same field range. This confirms the enhanced magnetic susceptibility resulting from the transformation of hematite to magnetite. Concurrently, a notable reduction in the distribution of SiO_2 and Al_2O_3 is observed across the whole magnetic induction range, with Na_2O levels being even lower, indicating improved selectivity. However, when ultrasound is applied in combination with reduction (Figure 11d), both the magnetic yield and the Fe_2O_3 recovery drop significantly at low field intensities—reaching only ~35% and ~40%, respectively, at 5 Gs—suggesting that ultrasound may interfere with early-stage capture of magnetic particles under weak fields. Nevertheless, as in the agitation-only cases, the magnetic fraction remains low in Na_2O, SiO_2, and Al_2O_3 content, confirming that selectivity is largely retained. Table 7 presents the chemical composition of the optimum, in terms of both Fe recovery and Fe grade, magnetic fractions obtained for both the non-reduced and reduced RBR and TBR samples under maximum field intensity. Upon reduction of the BR samples, the magnetic concentrates have a higher Fe grade and lower Al, in comparison to those obtained from the raw BR, due to the transformation of hematite to magnetite which enhances separation efficiency, and to the dissolution of residual Al in the alkaline solution.

Table 7. Chemical compositions (wt.%) of the optimum Fe grades for both non-reduced and reduced RBR and TBR magnetic fractions.

Origin and Conditions	Fe_2O_3	Al_2O_3	SiO_2	Na_2O	TiO_2	CaO	Other	LOI
Raw: non-reduced, Romanian Dispersion: Agitation Magnetic Field: 1600 Gs	42.5	17.2	10.9	6.5	2.8	2.0	1.8	16.3
Raw: reduced, Romanian Dispersion: Agitation Magnetic Field: 700 Gs	63.5	7.1	9.8	2.3	3.1	6.6	1.7	5.9
Raw: non-reduced, Turkish Dispersion: Agitation Magnetic Field: 1600 Gs	40.0	18.2	12.4	4.0	4.8	3.5	1.9	15.2
Raw: reduced, Turkish Dispersion: Agitation Magnetic Field: 700 Gs	46.6	9.9	13.4	5.7	4.9	7.0	1.7	10.8

3.4. Separation Performance

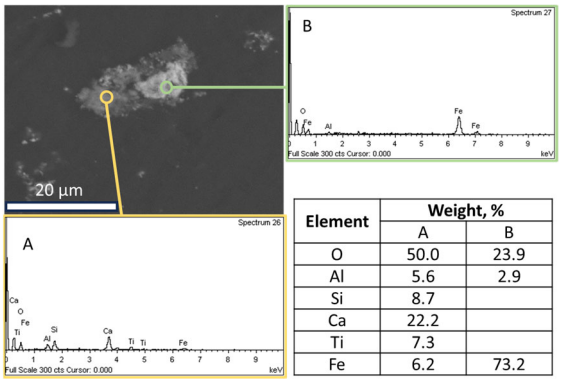
The separation of iron-containing phases from the bauxite residue appears to be influenced by several parameters, each affecting the process in distinct ways and to varying degrees:

- Hydrothermal treatment: the reduction of goethite and hematite and the formation of magnetite impacts the separation performance primarily because of the higher magnetic susceptibility of the latter. In addition to this, hydrothermal treatment reduces the mass of the solids due to Al leaching, leading to enrichment of the iron-containing minerals and those minerals containing Si, Na, Ca and Ti, evidenced by comparison of the composition of raw BR samples (Table 3) and the hydrothermally treated ones (Table 5). As has been shown elsewhere, the Al-rich liquor composition for Greek BR can have more than 17g/L Al_2O_3 [29]. With hydrothermal treatment, under a magnetic field of 400 Gs, the Fe recovery increases from 39.7% to 94.7% for

the RBR sample, and from 25.2% to 89.8% with hydrothermal treatment of the TBR sample. Fe grade increases too, but not so much; for the raw RBR, it increases from 30.2% to 44.6%, while for the TBR sample, it increases from 28.5% for raw BR to 32.8% for the concentrate obtained from the hydrothermally treated sample.

- Ultrasonication as particle dispersion method: the dispersion of the particles in the slurry that is fed into the magnetic separator is aimed at the breakage of agglomerates that would reduce the selectivity of the separation process. Indeed, as has been shown, the formation of the clusters is unavoidable due to the particle size. As seen in the SEM images (Figures 2, 3 and 5), a considerable portion of both the RBR and TBR samples consists of grains with sizes below 10 μm. With such a small particle size, attracting forces like surface tension, adhesion, and van der Waals forces dominate over gravity, promoting the production of clusters [29,35]. The application of ultrasounds combined with agitation for the dispersion of the particles in the slurry affected the magnetic fraction obtained; for separation under 400 Gs, the magnetic fraction is 36.1% under agitation and 21.8% when agitation and ultrasounds are combined for the raw Romanian sample; for the Turkish sample, the respective results are 24.4% and 14.1%. Ultrasound indeed broke the clusters, producing slurry with particles of lower effective diameters. This weakened the magnetic forces which are proportional to the size and allowed fluid forces (mainly drag) to prevail, enhancing the particles' entrainment by the water stream, as has been shown elsewhere [36]. Another explanation of the reduction in the separation performance under the application of ultrasound, is that, although ultrasonication improves particle dispersion, it also causes fracturing and cracking of the iron-containing bauxite residue particles [37]. As has been demonstrated, the presence of defects (such as cracks and gaps) within the particles leads to an increase in the internal demagnetizing field, which subsequently reduces the maximum magnetic permeability and retention efficiency [38].
- Sample origin: bauxite ore samples of different origins present differences in their chemical and mineralogical compositions [39]. As shown in Table 3, Romanian BR has a higher Fe content, while the Turkish one has higher contents of Si and Ti. As for the mineralogical composition of the sample, RBR contains considerable amounts of Al-boehmite and hematite while the TBR one has only hematite. Also, cancrinite is identified in the Turkish sample only, while the same sample has a higher gibbsite content as well. Among these minerals, hematite is considered antiferromagnetic at ambient temperature (below its Néel temperature of around 675 °C). Goethite is weakly ferromagnetic, and can potentially show weak ferromagnetic behavior; however, its magnetic susceptibility reduces significantly with the increasing substitution of Al, rendering it weakly paramagnetic [40]. On the other hand, magnetite has high magnetic susceptibility, rendering it easy for beneficiation through magnetic separation. However, as has been shown elsewhere, the mineral magnetic susceptibilities are weakly related to the mineral recoveries either in Wet Low Intensity or in Wet High Intensity Magnetic separation, with the particle size dictating the process for fine particles [41]. It is also important to consider the composition of the grains and whether the mineral phases are associated with others and to what degree. Figure 12 presents the SEM-EDS image of the treated RBR, together with the local chemical composition at two different locations of the same particle. The particle shows a distinct magnetite region, while the surrounding part of the particle has as complex multi-element composition of calcium silicate, Ti-minerals (perovskite or rutile) and minor Fe oxide inclusions of Fe substitution. These physicochemical characteristics reflect the difficulty of efficiently and selectively separating the iron-containing particles.

- Magnetic induction and composition of magnetic fractions: the applied magnetic field in combination with the nature of the iron phases (Fe^{3+} oxides or magnetite) affects the magnetic fraction mass produced, either for raw and for hydrothermally treated samples. It was found that for the Romanian sample at 1600 Gs, the magnetic fraction obtained after the separation is 55% of the feed, while after hydrothermal treatment, the application of 5 Gs is enough for the magnetic fraction to be 58.2% of the feed, with similar findings for the TBR material. An increase in the magnetic fraction mass is accompanied by an enhancement of the Fe recovery, while selective distribution of certain elements either in the magnetic and non-magnetic fraction was demonstrated. More specifically, the distribution of Ti in the magnetic concentrates is very similar to, and in some cases slightly higher than, that of Fe. This can be attributed to the close association of the Ti phases with Fe oxides, as was revealed via scanning electron microscopy (Figures 2, 3 and 5), as well as to the fact that Ti-bearing minerals exhibit only weak paramagnetic behavior, insufficient on its own to account for their retention during magnetic separation. Furthermore, a slight enrichment of the magnetic concentrate produced from the hydrothermally treated samples occurs for calcium. For the hydrothermally treated samples, Na_2O, SiO_2, and Al_2O_3 are distributed in the non-magnetic fraction which is attributed to their association with non-magnetic minerals.



Element	Weight, %	
	A	B
O	50.0	23.9
Al	5.6	2.9
Si	8.7	
Ca	22.2	
Ti	7.3	
Fe	6.2	73.2

Figure 12. SEM-EDS image of a particle of the hydrothermally treated RBR sample composed by a non-iron-rich (**A**) and an iron-rich (**B**) region. The respective EDS spectra and the elements com-positions are quoted.

4. Conclusions

In this research, two low-iron-grade bauxite residues from the alumina industries in Romania (RBR) and Turkey (TBR) were processed using hydrothermal reduction followed by wet magnetic separation. The initial residues contained Fe^{3+} oxides at comparable concentrations—approximately 39% in RBR and 35% in TBR. The Fe^{3+} oxides (hematite and goethite) were converted to magnetite with efficiencies of 76.7% and 49.9% after the hydrothermal processing of the RBR and TBR samples, respectively. The performance of the wet magnetic separation was better for the RBR sample, possibly due to its microstructural characteristics and reduced agglomeration phenomena. The optimal magnetic fraction obtained contained 44.4 wt.% elemental iron (Fe_{elem}), with an iron recovery of 98%. This represents a significant improvement compared to the magnetic fraction derived from the non-reduced samples, which showed a maximum of 29.7 wt.% Fe grade and 59.7% recovery. The achieved iron grade and recovery under optimum conditions (magnetic induction of 700 Gs and slurry dispersion through agitation) are generally comparable to those obtained from magnetic fractions produced by the separation of bauxite residues roasted under mild conditions according to the relative literature. The disintegration of particle clusters is more

effective when agitation is combined with ultrasound. However, this negatively affected iron recovery and grade which was attributed to the reduction in effective particle size and the enhanced influence of hydrodynamic forces at these finer size ranges.

Chemical analyses of the magnetic and non-magnetic fractions showed that the majority of the sodium—one of the main undesirable impurities for pig iron production—as well as the majority of the silicon were transferred to the non-magnetic fraction. Overall, the results are promising for the holistic valorization of bauxite residue, enabling the production of an iron concentrate rich in magnetite and the recycling of the aluminum-rich liquor back into the Bayer reactor. As future work, further intensification of the hydrothermal treatment to maximize the conversion degree, controlled grinding of the reduced samples to enhance the liberation of iron-containing phases, and reduction of pulp density during magnetic separation will merit investigation, with the aim of increase the iron content in the magnetic fraction.

Author Contributions: Conceptualization, P.A., P.O., G.A. and M.T.; investigation, P.A., P.O. and N.K.; resources, G.A. and M.T.; writing—original draft preparation, P.A., M.S. and N.K.; writing—review and editing, P.A. and M.S.; supervision, G.A. and M.T.; funding acquisition, M.T. All authors have read and agreed to the published version of the manuscript.

Funding: This research was implemented in the frame of the REEScue project (ID: 82, No. Project: 5122), which is funded by the ERA-NET Cofund on Raw Materials (ERA min 2), Funder: Horizon Europe 2020- European Commission (https://research-and-innovation.ec.europa.eu/funding/funding-opportunities/funding-programmes-and-open-calls/horizon-europe_en, accessed on 10 September 2025).

Data Availability Statement: The original contributions presented in this study are included in the article. Further inquiries can be directed to the corresponding author.

Acknowledgments: We acknowledge the support of personnel from Alum S.A., based in Tulcea, Romania, and Eti Alüminyum A.Ş., located in Seydişehir, Turkey, for kindly providing us the working samples. The authors have reviewed and edited the output and take full responsibility for the content of this publication.

Conflicts of Interest: The authors declare no conflicts of interest.

Abbreviations

The following abbreviations are used in this manuscript:

BR	Bauxite residue
RBR	Romanian bauxite residue
TBR	Turkish bauxite residue

References

1. Khairul, M.A.; Zanganeh, J.; Moghtaderi, B. The composition, recycling and utilisation of Bayer red mud. *Resour. Conserv. Recycl.* **2019**, *141*, 483–498. [CrossRef]
2. Sun, C.; Chen, J.; Tian, K.; Peng, D.; Liao, X.; Wu, X. Geochemical Characteristics and Toxic Elements in Alumina Refining Wastes and Leachates from Management Facilities. *Int. J. Environ. Res. Public Health* **2019**, *16*, 1297. [CrossRef]
3. Döring, J.; Beck, T.; Beyermann, M.; Gerlier, J.; Henze, G.; Mielcarek, J.; Schkade, U.-K. Exposure and radiation protection for work areas with enhanced natural radioactivity. In Proceedings of the Naturally Occurring Radioactive Material (NORM V), Seville, Spain, 19–22 March 2007.
4. Jovičević-Klug, M.; Souza Filho, I.R.; Springer, H.; Adam, C.; Raabe, D. Green steel from red mud through climate-neutral hydrogen plasma reduction. *Nature* **2024**, *625*, 703–709. [CrossRef]
5. International-Aluminium.org. Available online: https://international-aluminium.org/report-reveals-global-aluminium-demand-to-reach-new-highs-after-covid/#:~:text=Report%20Reveals%20Global%20Aluminium%20Demand,Mt%20and%20Europe%204.8Mt (accessed on 10 July 2025).

6. Archambo, M. New Horizons for Processing and Utilizing Red Mud. Ph.D. Thesis, School of Chemical Engineering, Michigan Technological University, Houghton, MI, USA, 2021.
7. Rai, S.; Bahadure, S.; Chaddha, M.J.; Agnihotri, A. Disposal practices and utilization of red mud (bauxite residue): A review in Indian context and abroad. *J. Sustain. Met.* **2019**, *6*, 1–8. [CrossRef]
8. CPCB Team. *Guidelines for Handling and Management of Red Mud Generated from Alumina Plants*; Central Pollution Control Board, Ministry of Environment, Forest and Climate Change: Delhi, India, 2023; p. 122.
9. Ruyters, S.; Mertens, J.; Vassilieva, E.; Dehandschutter, B.; Poffijn, A.; Smolders, E. The red mud accident in Ajka (Hungary): Plant toxicity and trace metal bioavailability in red mud contaminated soil. *Environ. Sci. Technol.* **2011**, *45*, 1616–1622. [CrossRef]
10. Reid, D.; Fourie, A.B. Back analyses of the August 2016 Luoyang red mud tailings failure. In Proceedings of the Tailings and Mine Waste Conference, Banff, AB, Canada, 5–8 November 2017.
11. Irfan-ul-Hassan, M.; Daud, M.; Rashid, K.; Alqahtani, F.K.; Zafar, I.; Batool, U. Development and sustainability assessment of red mud-based green bricks: Techno-economic and environmental performance. *J. Build. Eng.* **2024**, *95*, 110350. [CrossRef]
12. Liu, S.; Guan, X.; Zhang, S.; Dou, Z.; Feng, C.; Zhang, H.; Luo, S. Sintered bayer red mud based ceramic bricks: Microstructure evolution and alkalis immobilization mechanism. *Ceram. Int.* **2017**, *43*, 13004–13008. [CrossRef]
13. Kang, S.P.; Kwon, S.J. Effects of red mud and Alkali-Activated Slag Cement on efflorescence in cement mortar. *Constr. Build. Mater.* **2017**, *133*, 459–467. [CrossRef]
14. Kumar, A.; Saravanan, T.J.; Bisht, K.; Kabeer, K.I.S.A. A review on the utilization of red mud for the production of geopolymer and alkali activated concrete. *Constr. Build. Mater.* **2021**, *302*, 124170. [CrossRef]
15. Mukiza, E.; Zhang, L.L.; Liu, X.; Zhang, N. Utilization of red mud in road base and subgrade materials: A review. *Resour. Conserv. Recycl.* **2019**, *141*, 187–199. [CrossRef]
16. Pan, X.; Wu, H.; Lv, Z.; Yu, H.; Tu, G. Recovery of valuable metals from red mud: A comprehensive review. *Sci. Total Environ.* **2023**, *904*, 166686. [CrossRef]
17. Li, Y.; Wang, J.; Wang, X.; Wang, B.; Luan, Z. Feasibility study of iron mineral separation from red mud by high gradient superconducting magnetic separation. *Phys. C Supercond.* **2011**, *471*, 91–96. [CrossRef]
18. Yuan, S.; Wang, R.; Zhang, H.; Li, Y.; Liu, L.; Fu, Y. Investigation of mineral phase transformation technology followed by magnetic separation for recovery of iron values from red mud. *Sustainability* **2022**, *14*, 13787. [CrossRef]
19. Yu, J.; Li, Y.; Lv, Y.; Han, Y.; Gao, P. Recovery of iron from high-iron red mud using suspension magnetization roasting and magnetic separation. *Miner. Eng.* **2022**, *178*, 107394. [CrossRef]
20. Valeev, D.; Zinoveev, D.; Kondratiev, A.; Lubyanoi, D.; Pankratov, D. Reductive Smelting of Neutralized Red Mud for Iron Recovery and Produced Pig Iron for Heat-Resistant Castings. *Metals* **2019**, *10*, 32. [CrossRef]
21. Yang, X.; Chen, X.; Zhang, T.; Ye, J.; Lv, G.; Zhang, J. Study on reductive smelting of high-iron red mud for iron recovery. *Metals* **2022**, *12*, 639. [CrossRef]
22. Samouhos, M.; Taxiarchou, M.; Tsakiridis, P.E.; Potiriadis, K. Greek "red mud" residue: A study of microwave reductive roasting followed by magnetic separation for a metallic iron recovery process. *J. Hazar. Mater.* **2013**, *254–255*, 193–205. [CrossRef] [PubMed]
23. Agrawal, S.; Rayapudi, V.; Dhawan, N. Microwave Reduction of Red Mud for Recovery of Iron Values. *J. Sustain. Met.* **2018**, *4*, 427–436. [CrossRef]
24. Samouhos, M.; Taxiarchou, M.; Pilatos, G.; Tsakiridis, P.E.; Devlin, E.; Pissas, M. Controlled reduction of red mud by H_2 followed by magnetic separation. *Miner. Eng.* **2017**, *105*, 36–43. [CrossRef]
25. Sun, T.; Aslam, M.M.A.; Chen, G.; Peng, C. Low-temperature biomass pyrolytic reduction and recovery of iron oxides from red mud. *Miner. Eng.* **2025**, *222*, 109155. [CrossRef]
26. Grudinsky, P.; Zinoveev, D.; Yurtaeva, A.; Kondratiev, A.; Dyubanov, V.; Petelin, A. Iron Recovery from Red Mud Using Carbothermic Roasting with Addition of Alkaline Salts. *J. Sustain. Met.* **2021**, *7*, 858–873. [CrossRef]
27. Li, X.; Wang, Y.; Zhou, Q.; Qi, T.; Liu, G.; Peng, Z.; Wang, H. Transformation of hematite in diasporic bauxite during reductive Bayer digestion and recovery of iron. *Trans. Nonferrous Met. Soc. China* **2017**, *27*, 2715–2726. [CrossRef]
28. Pasechnik, L.A.; Skachkov, V.M.; Bogdanova, E.A.; Chufarov, A.Y.; Kellerman, D.G.; Medyankina, I.S.; Yatsenko, S.P. A promising process for transformation of hematite to magnetite with simultaneous dissolution of alumina from red mud in alkaline medium. *Hydrometallurgy* **2020**, *196*, 105438. [CrossRef]
29. Angelopoulos, P.M.; Oustadakis, P.; Anastassakis, G.; Pissas, M.; Taxiarchou, M. Iron recovery from bauxite residue (BR) through magnetic separation; Effect of endogenous properties and processing conditions. *Miner. Eng.* **2024**, *217*, 108954. [CrossRef]
30. Doebelin, N.; Kleeberg, R. Profex: A graphical user interface for the Rietveld refinement program BGMN. *J. Appl. Crystallogr.* **2015**, *48*, 1573–1580. [CrossRef]
31. Lu, J.F.; Tsai, C.J. Reduction kinetics of hematite to magnetite under hydrothermal treatments. *RSC Adv.* **2015**, *5*, 17236–17244. [CrossRef]
32. Simoni, M.; Hanein, T.; Woo, C.L.; Provis, J.; Kinoshita, H. Effect of impurities on the decarbonization of calcium carbonate using aqueous sodium hydroxide. *ACS Sustain. Chem. Eng.* **2022**, *10*, 11913–11925. [CrossRef]

33. Hellige, K. The Reactivity of Ferric (Hydr)Oxides Towards Dissolved Sulphide. Ph.D. Thesis, University of Bayreuth, Dortmund, Germany, 2010.
34. Yan, W.; Liu, H.; Chen, R.; Xie, J.; Wei, Y. Dissolution and oriented aggregation: Transformation from lepidorocite to goethite by the catalysis of aqueous Fe(II). *RSC Adv.* **2015**, *5*, 106396. [CrossRef]
35. Kendall, K. Adhesion: Molecules and Mechanics. *Science* **1994**, *263*, 1720–1725. [CrossRef] [PubMed]
36. Arol, A.I.; Aydogan, A. Recovery enhancement of magnetite fines in magnetic separation. *Colloids Surf. A Physicochem. Eng. Asp.* **2004**, *232*, 151–154. [CrossRef]
37. Hassanjani-Roshan, A.; Vaezi, M.R.; Koohestani, H.; Cheraghi, F. Investigating the Effect of Ultrasound Intensity on the Magnetic Properties of Magnetite Nanostructures Synthesized by Sonochemical Method. *Int. J. Eng.* **2023**, *36*, 1034–1039. [CrossRef]
38. Anhalt, M. Systematic investigation of particle size dependence of magnetic properties in soft magnetic composites. *J. Magn. Magn. Mater.* **2008**, *320*, 366–369. [CrossRef]
39. Angelopoulos, P.; Georgiou, M.; Oustadakis, P.; Taxiarchou, M.; Karadağ, H.; Eker, Y.; Dobra, G.; Boiangiu, A.; Demir, G.; Arslan, S.; et al. Preliminary Characterization of Three Metallurgical Bauxite Residue Samples. *Mater. Proc.* **2021**, *5*, 66.
40. Ponomar, V.P. Thermomagnetic properties of the goethite transformation during high-temperature treatment. *Miner. Eng.* **2018**, *127*, 143–152. [CrossRef]
41. Bazin, C.; Sista, R.; Légaré, B.; Caron, J.; Lavoie, F. Investigation of the effect of mineral composition and size on particle separation in Wet low and high intensities magnetic separators: An industrial case. *Miner. Eng.* **2024**, *218*, 109003. [CrossRef]

Disclaimer/Publisher's Note: The statements, opinions and data contained in all publications are solely those of the individual author(s) and contributor(s) and not of MDPI and/or the editor(s). MDPI and/or the editor(s) disclaim responsibility for any injury to people or property resulting from any ideas, methods, instructions or products referred to in the content.